2018

A Porous Media Model of Alveolar Duct Flow in the Human Lung

Anthony G. Straatman
uwo, agstraat@uwo.ca

Christopher T. DeGroot
Western University, cdegroo5@uwo.ca

A POROUS MEDIA MODEL OF ALVEOLAR DUCT FLOW IN THE HUMAN LUNG

Christopher T. DeGroot[*] *& Anthony G. Straatman*

Department of Mechanical and Materials Engineering, Western University, London, Ontario, N6A 5B9, Canada

[*]Address all correspondence to: Christopher T. DeGroot, Department of Mechanical and Materials Engineering, Western University, London, Ontario, N6A 5B9, Canada, E-mail: cdegroo5@uwo.ca

Prediction of air flow in the human lung is of great interest for many physiological applications. Recent advances in modeling such flows using computational fluid dynamics have included the development of porous media-based approaches that consider the small-scale airways and alveoli as a porous domain. This article presents a derivation of the governing equations relevant to flow in an alveolated duct based on the theory of volume-averaging as well as their closure. It is shown that the momentum closure problem reduces to that of a steady-state problem which is solved over a representative unit cell of an alveolated duct to predict its permeability. The modeling approach is validated against permeability predictions coming from transient simulations of flow in an expanding and contracting duct. Finally, analytical expressions for the velocity and pressure in an alveolated duct are derived and presented.

KEY WORDS: *respiratory flow, alveoli, closure modeling, permeability*

1. INTRODUCTION

Simulation of flow in the human lung is of interest because it can provide details of the flow that cannot be measured in vivo. Knowledge of the flow patterns within the lung are of practical importance because of the potential impacts on respiratory drug delivery, particle deposition, and our general understanding of the relationship between lung structure and function (Tawhai and Lin, 2010). The internal structure of the lung consists of a network of bifurcating airways that become smaller in both length and diameter with each subsequent bifurcation (or "generation"). The first sixteen generations are known as the conducting airways which take no part in the gas exchange process, but lead the air to the respiratory region of the lung (West, 2008). Gas exchange occurs by passive diffusion through the thin walls of small sacs, known as alveoli, which line the airways in the respiratory region, defined as the 17th generation and beyond (Weibel, 1963; West, 2008).

Simulating flow in the lung is particularly challenging due to the large number of flow paths and the wide range of length scales spanned by the various components of its structure. Airway diameters range from about 2 cm at the trachea to a fraction of a millimeter in the most distal airways (Weibel, 1963). There are approximately 300 million alveolar sacs in the human lung, each of which are about 0.3 mm in diameter (Weibel, 1963). Many computational fluid dynamics (CFD) studies have been conducted to study flow and particle deposition, as well as heat and mass transfer in the upper airways (Comerford et al., 2010; Gemci et al., 2008; Lin et al., 2009; Luo and Liu, 2008; Saksono et al., 2012; Tawhai and Lin, 2010; Walters and Luke, 2010, 2011; Yin et al., 2010; Zhang and Kleinstreuer, 2002, 2003; Zhang et al., 2008). Similarly, in the respiratory region, CFD simulations have been conducted to investigate the flow and particle transport in alveolated ducts (Harding and Robinson, 2010; Karl et al., 2004; Kumar et al., 2009, 2011; Lee and Lee, 2003; Li and Kleinstreuer, 2011; Ma and Darquenne, 2011; Sznitman et al., 2007, 2009; Tsuda et al., 2008). Although some attempts have been made to couple computational models of flow in the upper airways to models of flow in the lower airways (Comerford et al., 2010; Ma and Lutchen, 2006), the lower airway models employed in these studies are typically quite simplified.

NOMENCLATURE

A_{fe}	area in the fluid region on the boundary of an averaging volume (m^2)
A_{fs}	area at the intersection of V_f and V_s (m^2)
A	area (m^2)
D_H	hydraulic diameter (m)
$\mathbf{d}$	vector used in momentum closure (m)
$\mathbf{D}$	tensor used in momentum closure (m^2)
K	scalar permeability of porous medium (m^2)
$\mathbf{K}$	permeability tensor for porous medium (m^2)
ℓ	length scale of pore (m)
L	length scale of porous domain (m)
$\dot{m}$	mass flux (kg/s)
$\mathbf{n}_{fs}$	unit-normal vector directed from the fluid to solid phase
p	pressure (Pa)
$\tilde{p}$	pressure deviation (Pa)
t	time (s)
$\mathbf{u}$	fluid velocity vector ($= [u, v, w]$) (m/s)
$\tilde{\mathbf{u}}$	fluid velocity deviation vector ($= [\tilde{u}, \tilde{v}, \tilde{w}]$) (m/s)
U	characteristic velocity (m/s)
V	volume (m^3)

Wo	Womersley number
$\mathbf{x}$	position vector (m)
$\langle\,\rangle$	denotes extrinsic volume-average
$\langle\,\rangle^f$	denotes intrinsic volume-average with respect to the fluid constituent

Greek Symbols

Δ	denotes a change in a quantity
ε	porosity ($= V_f/V$)
Λ	amplitude
μ	dynamic viscosity (kg/m·s)
ρ	density (kg/m^3)
ϕ	generic scalar quantity
ω	angular frequency (rad/s)

Subscripts and Superscripts

0	initial value
$*$	denotes dimensionless quantity
f	fluid
in	inlet of periodic domain
s	solid
w	wall

It has been proposed by Owen and Lewis (2001), in their theoretical work on high-frequency ventilation, that the lung parenchyma can be modeled as a porous continuum. Using homogenization and volume-averaging, they developed a model to describe the flow and tissue deformation for small uniform samples of lung parenchyma. While the theoretical development of their model was well founded, it depended on several effective properties of the porous lung parenchyma that were only roughly estimated and only select one-dimensional results were obtained for the flow and tissue deformations. However, it was suggested that such a macroscopic description could be coupled with models for the upper airways. This provides a convenient way to simulate transport processes in the whole lung since full resolution in the upper airways can be obtained, while a coupled porous media model is used to account for the remainder of the airways and parenchyma. DeGroot and Straatman (2016) used this modeling concept and the method of volume averaging to develop a conjugate fluid-porous CFD model for the whole lung, where the upper airways were considered as a pure fluid region and the remainder of the lung volume was considered to be porous.

The goal of this work is to build upon the porous media concept for modeling air flow in the lung by considering the development and closure of the associated governing equations using the method of volume-averaging (Gray, 1975; Whitaker, 1967), which is then relatively straightforward to couple with models for the upper airways, as in DeGroot and Straatman (2016). The geometry of interest for this study is an expanding and contracting alveolated duct, as shown schematically in Fig. 1. Ultimately, it will be shown that the permeability of the duct is the only required closure parameter and that it can be obtained using a similar approach to Whitaker (1996). Results are presented to verify the model with respect to direct CFD calculations on the moving duct, followed by some one-dimensional results. The key outcomes of this work are the systematic development of the governing equations valid for an expanding/contracting porous medium relevant to respiratory flows and the permeability of the alveolated duct which can subsequently be used in combination with the governing equations to perform large-scale three-dimensional simulations of flow in the lung.
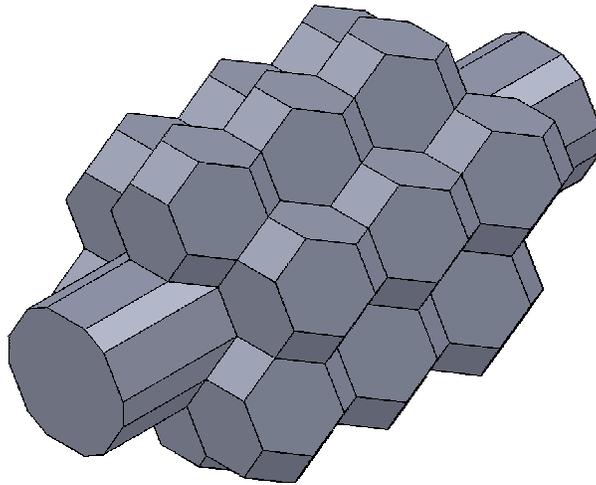
FIG. 1: A schematic diagram of an idealized geometric model of an alveolated duct

2. THEORETICAL MODEL

2.1 Governing Equations

Flow in the airway tree and alveoli is governed by the standard continuity and Navier-Stokes equations for an incompressible fluid, given by

$$\nabla \cdot \mathbf{u} = 0 \tag{1}$$

and

$$\rho_f \left(\frac{\partial \mathbf{u}}{\partial t} + \mathbf{u} \cdot \nabla \mathbf{u} \right) = -\nabla p + \mu_f \nabla^2 \mathbf{u}, \tag{2}$$

respectively, where $\mathbf{u}$ is the fluid velocity vector, p is the pressure, ρ_f is the fluid density, t is time, and μ_f is the fluid dynamic viscosity. Since there are far too many alveolar ducts in the human lung to consider directly, we average the above equations over a representative element of the lung parenchyma to obtain equations that can be solved for averaged quantities. For a porous medium composed of fluid and solid constituents, the definition of the extrinsic volume-average of a quantity ϕ_k is given by

$$\langle \phi_k \rangle = \frac{1}{V} \int_{V_k} \phi_k dV, \tag{3}$$

where $k \in \{f, s\}$ denotes the phase in which the quantity ϕ_k is defined with f and s indicating the fluid and solid phases, respectively. Note that V_f and V_s are the fluid and solid volumes, respectively, contained within the averaging volume V. The averaging volume V is considered fixed in space and of constant volume; however, the components V_f and V_s are free to change with time. For the purposes of this work, the air within the alveolated ducts represents the fluid phase while the tissue represents the solid phase. In addition to the extrinsic average, the intrinsic average is defined as

$$\langle \phi_k \rangle^k = \frac{1}{V_k} \int_{V_k} \phi_k dV, \tag{4}$$

which is an average over a single phase only. For the purposes of the theoretical development to follow, it is assumed that the porosity, $\varepsilon = V_f/V$, of the porous region may vary in both time and space. Following the procedure of Gray (1975) for the conditions outlined, the volume-averaged counterparts to Eqs. (1) and (2) are

$$\nabla \cdot \langle \mathbf{u} \rangle = -\frac{1}{V} \int_{A_{fs}(t)} \mathbf{u} \cdot \mathbf{n}_{fs} dA \tag{5}$$

and

$$\rho_f \left[\frac{\partial \langle \mathbf{u} \rangle}{\partial t} + \nabla \cdot \left(\frac{1}{\varepsilon} \langle \mathbf{u} \rangle \langle \mathbf{u} \rangle \right) \right] = -\varepsilon \nabla \langle p \rangle^f + \mu_f \nabla^2 \langle \mathbf{u} \rangle$$
$$+ \frac{1}{V} \int_{A_{fs}(t)} \left(-\tilde{p} \mathbf{n}_{fs} + \mu_f \nabla \tilde{\mathbf{u}} \cdot \mathbf{n}_{fs} \right) dA - \rho_f \nabla \cdot \langle \tilde{\mathbf{u}} \tilde{\mathbf{u}} \rangle, \tag{6}$$

respectively, where $A_{fs}(t)$ is the area of intersection between the fluid and solid volumes, V_f and V_s. The unit-normal vector directed from the fluid to solid phase on $A_{fs}(t)$ is denoted $\mathbf{n}_{fs}$. Spatial deviations are denoted, for a generic scalar ϕ, as $\tilde{\phi} = \phi - \langle \phi \rangle^f$. Note that A_{fs} is taken as a function of time since the walls of an alveolated duct are in motion as they expand and contract through the breathing cycle. For further details on the method of volume-averaging and the associated closure problem, see DeGroot and Straatman (2011a, 2012); Gray (1975); Kaviany (1995).

At this point, the forms of Eqs. (5) and (6) limit their use in practice due to the presence of surface integrals as well as terms depending on the pore-level spatial deviations $\tilde{p}$ and $\tilde{\mathbf{u}}$. In the sections to follow, these terms will be simplified such that the governing equations are closed; that is, they are cast in a form that is independent of pore-level quantities and all terms depend only on volume-averaged quantities.

2.2 Closure of Continuity Equation

The integral term appearing in the volume-averaged continuity equation, Eq. (5), may be treated simply on the basis that both the fluid and solid constituents are incompressible. First, let the fluid be bounded by the moving surface $A_{fs}(t) \cup A_{fe}(t)$, where $A_{fe}(t)$ is the portion of the fluid volume boundary which is not adjacent to the solid region and can therefore permit inflow and outflow. In terms of these bounding surfaces, the integral form of the continuity equation is given as

$$\int_{A_{fs}(t)} \mathbf{u} \cdot \mathbf{n}_{fs} dA + \int_{A_{fe}(t)} \mathbf{u} \cdot \mathbf{n}_{fs} dA = 0, \tag{7}$$

which expresses a balance between the changing size of the volume V_f due to the motion of the surface A_{fs} and the fluid that must be drawn in or expelled from the volume through A_{fe} in order to conserve mass. The second term on the left side of Eq. (7) represents the volume flux of fluid required to maintain a mass balance, with outflow being positive. This results in the expression

$$\int_{A_{fs}(t)} \mathbf{u} \cdot \mathbf{n}_{fs} dA = \frac{\partial V_f}{\partial t}. \tag{8}$$

Noting that $V_f = \varepsilon V$ and recalling that the averaging volume, V, is fixed in size, Eq. (8) may be combined with Eq. (5) to obtain the closed form of the continuity equation, given as

$$\nabla \cdot \langle \mathbf{u} \rangle = -\frac{\partial \varepsilon}{\partial t}. \tag{9}$$

2.3 Closure of Momentum Equation

To close Eq. (6), we follow the general approach of Whitaker (1996) in which transport equations for the spatial deviations are derived by subtracting the volume-averaged equations, appropriately scaled by porosity, from the continuum equation. In this case, however, there are additional terms arising from the fact that the porosity is allowed to vary in space and time, which will need to be considered.

The transport equation for the velocity deviations arising from the continuity equation is derived by subtracting Eq. (9), divided by ε, from Eq. (1). The result after some rearrangements is given as

$$\nabla \cdot \tilde{\mathbf{u}} = \frac{1}{\varepsilon} \frac{\partial \varepsilon}{\partial t} + \frac{1}{\varepsilon^2} \nabla \varepsilon \cdot \langle \mathbf{u} \rangle. \tag{10}$$

Compared to the equation of Whitaker (1996), Eq. (10) is quite complicated; however it can be shown through various scaling arguments that it can be simplified substantially, such that it is equivalent to that of Whitaker (1996), which is a desired outcome. The assumptions that are made for this analysis are summarized as follows:

(i) Variations in the velocity deviations, $\tilde{\mathbf{u}}$, occur over the length scale of the averaging volume with length scale ℓ, while variations in the volume-averaged velocity, $\langle \mathbf{u} \rangle$, and porosity, ε, occur over the length scale of the porous domain with length scale L; the length scale ℓ corresponds to the size of an alveolus, which has a length scale of approximately 0.3 mm (West, 2008) and L corresponds to the size of the lung which is $O(10^{-1}$ m$)$.

(ii) The velocity deviations and the volume-averaged velocity are of the same order, that is $\tilde{\mathbf{u}} \sim O(U)$ and $\langle \mathbf{u} \rangle \sim O(U)$, where U is a characteristic velocity; the characteristic velocity within an alveolated duct is $O(10^{-3}$ m/s$)$ (Ma and Darquenne, 2011).

(iii) The average porosity of the lung parenchyma is within the range $\bar{\varepsilon} = 0.7$ to 0.9 (Gehr et al., 1978; Kamschulte et al., 2013; Weibel, 1963), such that $\bar{\varepsilon} \sim O(1)$ and the deviation from this value is small ($\Delta\varepsilon \ll 1$).

(iv) The time scale of a breath cycle, t_b, is of the order of seconds; the time scale of the porosity variations is the same.

With these assumptions, which are all physiologically based, the order of magnitude of each of the terms in Eq. (10) may be estimated. On this basis of these assumptions it can be said that

$$\nabla \cdot \tilde{\mathbf{u}} \sim O\left(\frac{U}{\ell}\right) \sim O\left(10 \text{ s}^{-1}\right), \tag{11a}$$

$$\frac{1}{\varepsilon}\frac{\partial\varepsilon}{\partial t} \sim O\left(\frac{\Delta\varepsilon}{\bar{\varepsilon}t_b}\right), \tag{11b}$$

$$\frac{1}{\varepsilon^2}\nabla\varepsilon \cdot \langle \mathbf{u} \rangle \sim O\left(\frac{\Delta\varepsilon U}{\bar{\varepsilon}^2 L}\right). \tag{11c}$$

The order of magnitude of the term listed in Eq. (11b) is proportional to the ratio $\Delta\varepsilon/\bar{\varepsilon}$, divided by the time scale, t_b, which is of the order of seconds according to assumption (iv). It has already been stated that the variation in porosity, $\Delta\varepsilon$, is much less than 1 and that the average porosity, $\bar{\varepsilon}$, is close to 1. Provided $\Delta\varepsilon$ is at least one order of magnitude smaller than ε it can be shown that the order of magnitude of this term is no more than 10^{-1} s^{-1}, or at least two orders smaller than the term listed in Eq. (11a). As a result, the term on the left side of Eq. (10) has been found to be much larger than the first term on the right, given the assumptions above, and may be neglected in this analysis.

Based on the magnitude of the velocity given in assumption (ii) and the characteristic length given in assumption (i), the order of magnitude of the term given in Eq. (11c) is of the order 10^{-2} s^{-1} multiplied by the ratio $\Delta\varepsilon/\bar{\varepsilon}^2$, which is also smaller than 1. Therefore it is clear that the term given in Eq. (11c) is much smaller than the term given in Eq. (11a). As a result, the last term on the right side of Eq. (10) may also be neglected in comparison to the term on the left.

With these simplifications, the transport equation for the velocity deviations, arising from the continuity equations, is

$$\nabla \cdot \tilde{\mathbf{u}} = 0, \tag{12}$$

as in the analysis of Whitaker (1996) for rigid porous solids.

The transport equation for the spatial deviations arising from the momentum equations is derived by subtracting Eq. (6), divided by ε, from Eq. (2). This results in

$$
\begin{aligned}
\rho_f \left(\frac{\partial \tilde{\mathbf{u}}}{\partial t} - \frac{1}{\varepsilon^2} \frac{\partial \varepsilon}{\partial t} \langle \mathbf{u} \rangle + \mathbf{u} \cdot \nabla \tilde{\mathbf{u}} + \tilde{\mathbf{u}} \cdot \nabla \langle \mathbf{u} \rangle^f - \frac{\nabla \varepsilon}{\varepsilon} \cdot \langle \mathbf{u} \rangle^f \langle \mathbf{u} \rangle^f \right) &= -\nabla \tilde{p} + \mu_f \nabla^2 \tilde{\mathbf{u}} \\
- \mu_f \langle \mathbf{u} \rangle \left(\frac{\nabla^2 \varepsilon}{\varepsilon} - \frac{2 \nabla \varepsilon \cdot \nabla \varepsilon}{\varepsilon^2} \right) - \mu_f \frac{2 \nabla \varepsilon}{\varepsilon} \nabla \langle \mathbf{u} \rangle - \frac{1}{V_f} \int_{A_{fs}(t)} & \left(-\tilde{p} \mathbf{n}_{fs} + \mu_f \nabla \tilde{\mathbf{u}} \cdot \mathbf{n}_{fs} \right) dA \\
+ \frac{\rho_f}{\varepsilon} \nabla \cdot \langle \tilde{\mathbf{u}} \tilde{\mathbf{u}} \rangle, &
\end{aligned}
\tag{13}
$$

after much algebraic simplification. Let us first examine the orders of magnitude of the terms on the left side of Eq. (13), under the assumptions listed previously. These are listed as

$$
\frac{\partial \tilde{\mathbf{u}}}{\partial t} \sim O \left(\frac{U}{t_b} \right),
\tag{14a}
$$

$$
\frac{1}{\varepsilon^2} \frac{\partial \varepsilon}{\partial t} \langle \mathbf{u} \rangle \sim O \left(\frac{\Delta \varepsilon U}{t_b} \right),
\tag{14b}
$$

$$
\mathbf{u} \cdot \nabla \tilde{\mathbf{u}} \sim O \left(\frac{U^2}{\ell} \right),
\tag{14c}
$$

$$
\tilde{\mathbf{u}} \cdot \nabla \langle \mathbf{u} \rangle^f \sim O \left(\frac{U^2}{L} \right),
\tag{14d}
$$

$$
\frac{\nabla \varepsilon}{\varepsilon} \cdot \langle \mathbf{u} \rangle^f \langle \mathbf{u} \rangle^f \sim O \left(\frac{\Delta \varepsilon U^2}{L} \right).
\tag{14e}
$$

Since $\ell \ll L$ and $\Delta \varepsilon \ll 1$, the terms given in Eqs. (14d) and (14e) are negligible in comparison to the term given in Eq. (14c). As stated previously, U/ℓ is of the order of 10 s^{-1} and the characteristic time scale, t_b, is of the order of 1 s. Thus, the term in Eq. (14a) is an order of magnitude smaller than the term in Eq. (14c), which is deemed small enough that it may be neglected. Since $\Delta \varepsilon \ll 1$, the term in Eq. (14b) is much less than the term in Eq. (14a), so this term may also be neglected in comparison to that in Eq. (14c). Therefore, of all the terms on the left side of Eq. (13), only the third survives. Then, since

$$
\frac{1}{\varepsilon} \nabla \cdot \langle \tilde{\mathbf{u}} \tilde{\mathbf{u}} \rangle \sim O \left(\frac{U^2}{L} \right),
\tag{15}
$$

the final term on the right side of Eq. (13) may be neglected in comparison to the surviving term on the left side.

The additional viscous terms, arising from the fact that the porosity is assumed to be spatially varying, can also be simplified. Since we have

$$
\nabla^2 \tilde{\mathbf{u}} \sim O \left(\frac{U}{\ell^2} \right),
\tag{16a}
$$

$$
\frac{\langle \mathbf{u} \rangle \nabla^2 \varepsilon}{\varepsilon} \sim O \left(\frac{U \Delta \varepsilon}{L^2} \right),
\tag{16b}
$$

$$
\frac{\langle \mathbf{u} \rangle \nabla^2 \varepsilon}{\varepsilon} \sim O \left(\frac{U (\Delta \varepsilon)^2}{L^2} \right),
\tag{16c}
$$

$$
\frac{\nabla \varepsilon}{\varepsilon} \nabla \langle \mathbf{u} \rangle \sim O \left(\frac{U \Delta \varepsilon}{L^2} \right),
\tag{16d}
$$

and since $\ell \ll L$ and $\Delta\varepsilon \ll 1$, we can neglect all but the first viscous term, which is listed in Eq. (16a). With these simplifications, the transport equation for the velocity and pressure deviations given by Whitaker (1996) is recovered. This is given as

$$\rho_f \mathbf{u} \cdot \nabla\tilde{\mathbf{u}} = -\nabla\tilde{p} + \mu_f \nabla^2\tilde{\mathbf{u}} - \frac{1}{V_f} \int_{A_{fs}(t)} (-\tilde{p}\mathbf{n}_{fs} + \mu_f \nabla\tilde{\mathbf{u}} \cdot \mathbf{n}_{fs})\, dA. \tag{17}$$

The fact that the transport equation for steady problems with constant porosity is recovered is significant because it means that one may neglect any time dependence as well as any porosity variations when considering the pore-scale closure problem, under the assumptions given previously for air flow in an alveolated duct. This is quite advantageous since these additional terms would be quite challenging to deal with in a general way. Fortunately, under these limiting conditions, the transport equations for the spatial deviations reduce to those of Whitaker (1996) and we may use the closure method proposed in that work. In fact, since the Reynolds number in alveolar flows is very low, one can further show that the convective term on the left side of Eq. (17) may also be neglected, resulting in the final form of the transport equation for the velocity and pressure deviations, given as

$$0 = -\nabla\tilde{p} + \mu_f \nabla^2\tilde{\mathbf{u}} - \frac{1}{V_f} \int_{A_{fs}(t)} (-\tilde{p}\mathbf{n}_{fs} + \mu_f \nabla\tilde{\mathbf{u}} \cdot \mathbf{n}_{fs})\, dA. \tag{18}$$

Next, the boundary conditions on Eqs. (12) and (18) must be considered. On the moving walls of the alveolated duct, the velocity deviation is expressed as $\tilde{\mathbf{u}} = \mathbf{u} - \langle\mathbf{u}\rangle^f$. Since the wall displacement over a breath cycle is $O(10^{-5}$ m) over a time scale that is $O(1$ s), the wall velocity can be estimated as $O(10^{-5}$ m/s), which is considered negligible in comparison to the bulk velocity which is typically $O(10^{-3}$ m/s). Additionally, although the velocity field is not strictly periodic due to the volume flow into the expanding alveoli, a periodic condition can still be considered appropriate since the volume flow rate into the alveoli is typically less than 1% of that in the alveolar duct (Kumar et al., 2009). Thus, it has been shown that wall motion can be neglected within the context of the pore-level closure problem. In summary, the boundary conditions on the velocity and pressure deviations are given as

$$\tilde{\mathbf{u}} = -\langle\mathbf{u}\rangle^f, \text{ on } A_{fs}, \tag{19a}$$

$$\tilde{\mathbf{u}}(\mathbf{x}_{in} + \Delta\mathbf{x}) = \tilde{\mathbf{u}}(\mathbf{x}_{in}), \text{ on } A_{fe}, \tag{19b}$$

$$\tilde{p}(\mathbf{x}_{in} + \Delta\mathbf{x}) = \tilde{p}(\mathbf{x}_{in}), \text{ on } A_{fe}, \tag{19c}$$

where the conditions given in Eqs. (19b) and (19c) express the periodicity of the flow between an inflow point $\mathbf{x}_{in}$ on $A_{fe}(t)$ and the corresponding outflow location $\mathbf{x}_{in} + \Delta\mathbf{x}$. Figure 2 shows a periodic unit of an alveolated duct upon which the boundary conditions above may be applied. Note that A_{fs} and A_{fe} are no longer considered functions of time since it has been shown that the boundary motion can be neglected within the closure problem.

To derive the closure problem, which is to be solved on the appropriate periodic unit cell, we first redefine the additional integral term remaining in Eq. (6) in terms of the permeability tensor $\mathbf{K}$ according to

$$\frac{1}{V} \int_{A_{fs}(t)} (-\tilde{p}\mathbf{n}_{fs} + \mu_f \nabla\tilde{\mathbf{u}} \cdot \mathbf{n}_{fs})\, dA = \varepsilon\mu_f \mathbf{K}^{-1} \cdot \langle\mathbf{u}\rangle. \tag{20}$$

Then, based on a series of variable transformations that are further described in Whitaker (1996) and DeGroot and Straatman (2012), the following closure problem is derived, to be solved on the periodic unit cell.

$$\nabla \cdot \mathbf{D} = 0, \tag{21a}$$

$$-\nabla\mathbf{d} + \nabla^2\mathbf{D} + \mathbf{I} = 0, \tag{21b}$$

subject to the boundary conditions,

$$\mathbf{D} = 0, \text{ on } A_{fs}, \tag{22a}$$

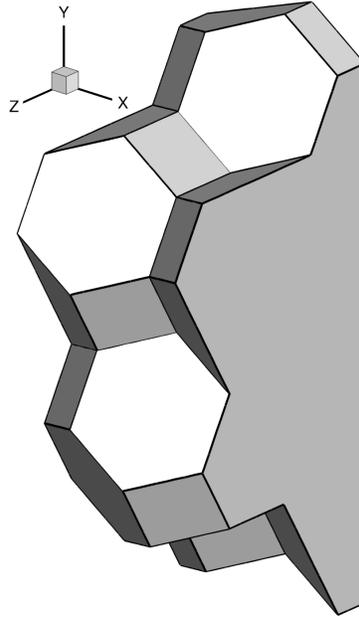$$\mathbf{D}(\mathbf{x}_{in} + \Delta\mathbf{x}) = \mathbf{D}(\mathbf{x}_{in}), \text{ on } A_{fe}, \tag{22b}$$

FIG. 2: A schematic diagram of a periodic unit cell of the idealized geometric model of an alveolated duct

$$\mathbf{d}(\mathbf{x}_{in} + \Delta\mathbf{x}) = \mathbf{d}(\mathbf{x}_{in}), \text{ on } A_{fe}. \tag{22c}$$

Now, Eqs. (21a) and (21b) may be solved along with the conditions listed in Eqs. (22a)–(22c) to determine the permeability tensor as

$$\mathbf{K} = \varepsilon\langle\mathbf{D}\rangle^f. \tag{23}$$

Note that for a general deforming domain, $\mathbf{K}$ is a function of the pore geometry and thus a function of time. For general motions, this would require evaluation of $\mathbf{K}$ for each required configuration; however, as will be seen, the characterization of $\mathbf{K}$ as a function of time is simplified for motions where the domain is simply scaled as is typically assumed for alveolated duct flows.

With the definition of the permeability, the closed form of the volume-averaged momentum equation is then given by

$$\rho_f\left[\frac{\partial\langle\mathbf{u}\rangle}{\partial t} + \nabla\cdot\left(\frac{1}{\varepsilon}\langle\mathbf{u}\rangle\langle\mathbf{u}\rangle\right)\right] = -\varepsilon\nabla\langle p\rangle^f + \mu_f\nabla^2\langle\mathbf{u}\rangle - \varepsilon\mu_f\mathbf{K}^{-1}\cdot\langle\mathbf{u}\rangle, \tag{24}$$

where the final term in Eq. (6) has been neglected due to periodicity. Note that although it was found that transient and porosity gradient effects may be neglected at the pore level, such effects may still be taken into account at the volume-averaged level through the closed volume-averaged momentum equation, Eq. (24).

3. RESULTS AND DISCUSSION

3.1 Permeability Tensor

For flow in a duct where the bulk flow is in the x direction and the walls are impermeable, the permeability tensor takes on the general form

$$\mathbf{K} = \begin{bmatrix} K & 0 & 0 \\ 0 & 0 & 0 \\ 0 & 0 & 0 \end{bmatrix}, \tag{25}$$

where K is the scalar permeability in the x direction, since bulk flow transverse to the duct axis is not permitted. From a numerical perspective, however, this form poses a problem since the matrix given in Eq. (25) is clearly noninvertible. Thus, we assume that the diagonal elements which take on a value of zero are instead equal to $1/a$, where a is an arbitrarily large value. Thus, the inverse of the permeability tensor may be computed as

$$\mathbf{K}^{-1} = \begin{bmatrix} 1/K & 0 & 0 \\ 0 & a & 0 \\ 0 & 0 & a \end{bmatrix}, \tag{26}$$

which, according to the closed volume-averaged momentum equation given in Eq. (24), prevents any bulk flow transverse to the axis of the duct through the very large Darcy term in these directions. Note that some care must be taken in selecting a to ensure that it is sufficiently large to serve its purpose, but not so large that it causes numerical difficulties.

Results for the permeability tensor are obtained by numerically solving Eqs. (21)–(22) using an in-house finite-volume-based computational fluid dynamics code (DeGroot and Straatman, 2011b, 2012) and integrating the results according to Eq. (23). The domain under consideration is a periodic unit cell representing the idealized alveolated duct geometry shown in Fig. 1, which was previously used by Kumar et al. (2009, 2011). The unit-cell geometry, taking into account the symmetry about a central plane, is shown in Fig. 2. Note that to solve the permeability using the proposed model requires only a single numerical solution of Eqs. (21) and (22). A grid resolution study indicated that a computational grid containing 244,331 tetrahedral volumes, refined towards walls, was sufficient to obtain a permeability tensor that is independent of the grid to less than 1% upon doubling the total number of control volumes in the domain.

To promote generality of the results, the computed scalar permeability K is presented in dimensionless form as $K/(\varepsilon D_H^2)$, where D_H is the hydraulic diameter of the central duct. Scaling the results by the hydraulic diameter is convenient because it allows the time-varying nature of the volume-averaged flow to be simplified as a time-varying permeability where the dimensionless permeability is constant but the hydraulic diameter of the duct changes. The permeability is also scaled by the porosity since we do not wish to specify a particular porosity for this model, since the choice of porosity depends on the nature of the system being modeled at a volume-averaged level. Numerical results confirm the form of the permeability tensor given in Eq. (25) and show that $K/(\varepsilon D_H^2) = 9.46 \times 10^{-3}$.

3.2 Verification of the Porous Media Model

In order to verify the proposed porous media model of flow in an alveolated duct and the validity of the assumptions underlying the theoretical basis of the model, transient simulations were conducted using ANSYS® CFX, Release 13.0, to compare the model predictions with direct CFD calculations in an expanding and contracting alveolar duct geometry. A one-dimensional version of Eq. (24), neglecting any macroscopic velocity gradients, results in

$$\rho_f \frac{\partial \langle u \rangle^f}{\partial t} = -\frac{\partial \langle p \rangle^f}{\partial x} - \frac{\varepsilon \mu_f \langle u \rangle^f}{K}, \tag{27}$$

where all averages have been converted to intrinsic averages and a constant porosity is assumed for the purposes of this verification exercise. Multiplying Eq. (27) by D_H^2 and solving for $K/(\varepsilon D_H^2)$ results in

$$\frac{K}{\varepsilon D_H^2} = \frac{\mu_f \langle u \rangle^f}{D_H^2} \left[-\frac{d \langle p \rangle^f}{dx} - \rho_f \frac{\partial \langle u \rangle^f}{\partial t} \right]^{-1}, \tag{28}$$

where the terms on the right side of Eq. (28) may be obtained directly from CFD calculations to verify that the results match the modeled $K/(\varepsilon D_H^2)$ expression, and that the averaging procedure is correctly capturing the hydrodynamics.

The CFD calculations are conducted using the full alveolated duct geometry shown in Fig. 1. At the inlet a uniform velocity profile was specified such that the Reynolds number based on the hydraulic diameter of the duct was $\mathrm{Re}_{D_H} = 0.01$ in the initial undeformed geometry. At the outlet a specified average static pressure of zero was imposed. At all other walls, the velocity was taken to be the velocity of the walls, i.e., a no-slip, no-penetration

condition relative to the walls. All boundary surfaces were moved as a simple sinusoidal scaling of the domain, according to

$$\mathbf{x}(t) = \mathbf{x}_0[1 + \Lambda_w \sin(\omega t)], \qquad (29)$$

where $\mathbf{x}(t)$ is the position of a point at time t, $\mathbf{x}_0$ is the location of the corresponding point in its initial configuration at time $t = 0$, Λ_w is the dimensionless amplitude of the wall motion, and ω is the angular frequency of the motion. At this juncture, it is useful to relate the dimensionless amplitude Λ_w to the relative change in the fluid volume, which is more easily related to physiological measurements. Since the overall dimensions of the alveolated duct, according to Eq. (29), will change by a factor of $(1 + \Lambda_w)/(1 - \Lambda_w)$ from its fully contracted to fully expanded states, the relative change in fluid volume is given as

$$\frac{V_{f,\max}}{V_{f,\min}} = \left(\frac{1 + \Lambda_w}{1 - \Lambda_w}\right)^3, \qquad (30)$$

where $V_{f,\min}$ and $V_{f,\max}$ are the minimum and maximum amounts of fluid present within the breath cycle, respectively. For the cases considered here, the dimensionless amplitude of the motion is taken to be $\Lambda_w = 1/2^n$ where $n \in \{2, 3, 4, 5, 6\}$ which results in relative volume changes, $V_{f,\max}/V_{f,\min}$, in the range 1.10–4.63. This range is selected such that it encompasses the typical physiological value of approximately 15% volumetric expansion during the breath cycle (Harding and Robinson, 2010) and extends far beyond this value to explore the range of applicability for the modeling assumptions introduced. The angular frequency is taken such that the Womersley number is Wo = 0.01 (Wo = $D_{H,0}/2\sqrt{\rho_f \omega/\mu_f}$, where $D_{H,0}$ is the hydraulic diameter of the main duct in its initial configuration at time $t = 0$). This value is motivated by the fact that $D_{H,0} \sim O(10^{-4} \text{ m})$ and that $\omega \sim O(1 \text{ rad/s})$, along with the viscosity of air, which results in an order of magnitude Wo $\sim O(0.01)$.

Note that the choice of parameters for these verification cases is not motivated by the study of a specific physiological process, rather we seek to choose parameters that are of the correct magnitude for the process of breathing to test the modeling assumptions. For example, we do not claim that a constant velocity imposed at the entrance of the alveolated duct necessarily represents the breathing process as it occurs physiologically, rather it represents a simplified problem with the correct magnitude of the key parameters such that the assumptions of the model may be tested.

To compare the predicted value of the dimensionless permeability coming from the solution of the closure problem with those coming from the direct CFD calculation, Eq. (28) is evaluated at each time step of the CFD simulation by appropriately averaging the solution field. The differences between the value predicted from the closure problem in comparison to those obtained from the transient CFD simulations are summarized in Table 1 in terms of an average error and a maximum error across all time steps. These results indicate that the value of the dimensionless permeability calculated from the closure problem matches well with the value obtained directly from the transient CFD simulations conducted in the alveolated duct, even for amplitudes of motion that are far in excess of what would be observed physiologically. In all cases, the average percent error is less than 2%. For the cases within the expected physiological range for the amplitude of motion, the average percent error is less than 1%. The maximum percent error is found to be less than 2% for the cases within the expected physiological range of Λ_w. For the higher-amplitude

TABLE 1: Summary of the maximum and average percent errors between the modeled value of $K/(\varepsilon D_H^2)$ and the value obtained using transient simulations in an alveolated duct and Eq. (28)

Λ_w	Max. % Error	Avg. % Error
1/64	1.4	0.71
1/32	1.5	0.79
1/16	1.6	0.91
1/8	2.5	1.0
1/4	4.5	1.9

cases, the error increases, but given the combined discretization errors of the permeability calculation and the direct CFD calculation, and the fact that the amplitude of motion is so large, this agreement is in fact quite satisfactory. Note that the second term on the right side of Eq. (28), i.e., the transient term, was generally found to be negligible in the CFD simulation; therefore the verification exercise has effectively shown that the pressure gradient estimated by direct CFD calculations matches with that predicted using the proposed permeability model, and that the averaging procedure is valid.

Overall, considering that the simplified porous media model, which requires only fairly basic calculations to solve, is able to match the results of a complex CFD calculation to within less than 5%, even for an excessively large amplitude of motion, the utility of this method of analysis is clear. Taking these results together implies that the theoretical development proposed in this work is indeed sound and that transient effects can be neglected within the closure problems. Further it shows that the impact of the alveolar expansion on the permeability is conveniently characterized through nondimensionalization by the hydraulic diameter such that $K/(\varepsilon D_H^2)$ is a constant value throughout the transient expansion/contraction process as D_H changes.

3.3 Validation of the Porous Media Model

Complete validation of the porous media is complicated, due to the complexities of taking experimental measurements of pressure and velocity in the lung parenchyma. That being said, the model has been partially validated to show that when implemented into a full porous media model of the human lung, the total pressure drop is of the correct order of magnitude. The permeability model described in this work has been previously implemented in conjugate simulations of airflow in the human lung by DeGroot and Straatman (2016). In that work it was shown that the overall pressure drop from inlet to the most distal airways was just more than 0.5 cm H_2O which compared reasonably well with a value of 1 cm H_2O for normal breathing reported by West (2008). It should be taken into consideration that the simulations of DeGroot and Straatman (2016) were conducted for about 80% of the normal tidal volume for breathing, so the pressure drop would be expected to be somewhat smaller. Other factors that should be further investigated include the specification of the diaphragm motion and the porosity distribution.

3.4 One-Dimensional Results for Flow in an Alveolated Duct

In this section, results are presented for one-dimensional flow in an alveolated duct, up to a terminal alveolus. In one dimension, the volume-averaged continuity equation, Eq. (9), reduces to

$$\frac{\partial \langle u \rangle}{\partial x} = -\frac{\partial \varepsilon}{\partial t}, \tag{31}$$

while the volume-averaged momentum equation, Eq. (24) reduces to

$$\rho_f \left[\frac{\partial \langle u \rangle}{\partial t} + \frac{2\langle u \rangle}{\varepsilon} \frac{\partial \langle u \rangle}{\partial x} \right] = -\varepsilon \frac{\partial \langle p \rangle^f}{\partial x} + \mu_f \frac{\partial^2 \langle u \rangle}{\partial x^2} - \frac{\varepsilon \mu_f \langle u \rangle}{K}, \tag{32}$$

where the porosity is considered to be a function of time, but constant in space for the purposes of this analysis. Defining the dimensionless groups,

$$x^* = \frac{x}{D_{H,0}}, \tag{33a}$$

$$u^* = \frac{\langle u \rangle}{\omega D_{H,0}}, \tag{33b}$$

$$p^* = \frac{\langle p \rangle^f}{\rho_f \omega^2 D_{H,0}^2}, \tag{33c}$$

$$t^* = \frac{\omega t}{2\pi}. \tag{33d}$$

Equations (9) and (32) become

$$\frac{\partial u^*}{\partial x^*} = -\frac{1}{2\pi}\frac{\partial \varepsilon}{\partial t^*} \tag{34}$$

and

$$\frac{1}{2\pi}\frac{\partial u^*}{\partial t^*} + \frac{2u^*}{\varepsilon}\frac{\partial u^*}{\partial x^*} = -\varepsilon\frac{\partial p^*}{\partial x^*} + \frac{1}{4\text{Wo}^2}\frac{\partial^2 u^*}{\partial x^{*2}} - \frac{1}{4\text{Wo}^2 K_0}\left(\frac{D_{H,0}}{D_H}\right)^2 u^*, \tag{35}$$

respectively, where

$$\text{Wo} = \frac{D_{H,0}}{2}\sqrt{\frac{\rho_f \omega}{\mu_f}} \tag{36}$$

is the Womersley number and $K_0 = K/(\varepsilon D_H^2)$ is the value of the dimensionless permeability obtained from the pore-level closure problem. To solve the problem described above, the porosity and hydraulic diameter of the duct must be known as functions of time in order to properly define all of the parameters appearing in Eqs. (34) and (35). In accordance with the scaling given by Eq. (29) the hydraulic diameter varies according to

$$\frac{D_H(t^*)}{D_{H,0}} = 1 + \Lambda_w \sin(2\pi t^*), \tag{37}$$

where $D_{H,0}$ is the hydraulic diameter at $t = 0$, corresponding to the mean length scale. To estimate the variation of porosity with respect to time, we begin with the assumption that the solid (tissue) volume does not change since it is incompressible (Owen and Lewis, 2001) which leads to the conclusion that the solid volume is given as

$$V_s = V_{f,0}\left(\frac{1-\varepsilon_0}{\varepsilon_0}\right) \tag{38}$$

for all time, where ε_0 is the porosity at the mean length scale. Noting that the fluid volume varies according to $V_f = V_{f,0}[1 + \Lambda_w \sin(2\pi t^*)]^3$ and using this in the definition of the porosity results in

$$\varepsilon(t^*) = \frac{\varepsilon_0(1 + \Lambda_w \sin(2\pi t^*))^3}{\varepsilon_0\left[(1 + \Lambda_w \sin(2\pi t^*))^3 - 1\right] + 1} \tag{39}$$

and

$$\frac{\partial \varepsilon}{\partial t^*} = -\frac{6\pi\varepsilon_0\left(\varepsilon_0 - 1\right)\Lambda_w \cos\left(2\pi t^*\right)\left[1 + \Lambda_w \sin\left(2\pi t^*\right)\right]^2}{\left[3\varepsilon_0\Lambda_w \sin\left(2\pi t^*\right) + 3\varepsilon_0\Lambda_w^2\left(\sin\left(2\pi t^*\right)\right)^2 + \varepsilon_0\Lambda_w^3\left(\sin\left(2\pi t^*\right)\right)^3 + 1\right]^2} \tag{40}$$

Results are to be obtained for an alveolated duct, where at $x^* = 0$ there is a terminal alveolus such that $u^* = 0$ and the pressure is the alveolar pressure p_a, which is referenced to zero. Solving Eq. (34) with the boundary condition $u^* = 0$ at $x^* = 0$ results in a solution for u^* as

$$u^*(x^*, t^*) = -\frac{1}{2\pi}\frac{\partial \varepsilon}{\partial t^*}x^*, \tag{41}$$

where $\partial\varepsilon/\partial t^*$ is obtained from Eq. (40). This result shows that the velocity is linear in x^* such that the viscous term in Eq. (35) is zero, and the equation for $\partial p^*/\partial x^*$ can be reduced to

$$\frac{\partial p^*}{\partial x^*} = -\frac{1}{\varepsilon}\left[\frac{1}{2\pi}\frac{\partial u^*}{\partial t^*} + \frac{2u^*}{\varepsilon}\frac{\partial u^*}{\partial x^*} + \frac{1}{4\text{Wo}^2 K_0}\left(\frac{D_{H,0}}{D_H}\right)^2 u^*\right], \tag{42}$$

where all quantities on the right side of Eq. (42) are known for a given time, such that it can be numerically integrated to obtain pressure profiles for given instants in time. The initial Womersley number, i.e., the Womersley number at time $t^* = 0$, is taken to be Wo = 0.01, which roughly corresponds to a normal breathing rate and average alveolar duct dimensions. The initial porosity is taken to be $\varepsilon_0 = 0.8$, which is a typical value for the lung parenchyma (DeGroot

and Straatman, 2016; Gehr et al., 1978; Kamschulte et al., 2013; Weibel, 1963). The amplitude of the wall motion is taken to be $\Lambda_w = 0.02329$, yielding a typical 15% expansion in the fluid volume (Harding and Robinson, 2010; Sznitman et al., 2009). Using these parameters, the dimensionless velocity profile can be obtained from Eq. (41) and the pressure profile can be obtained by integrating Eq. (42) with respect to x^*. In this case, integration is performed using a variable-step Runge-Kutta method, although numerical experiments revealed that only the last term in Eq. (42) was significant for the parameters chosen for these cases. Therefore, subsequent results were simply obtained using the analytical expression for the pressure, given by

$$p^* = (16\pi\varepsilon\mathrm{Wo}^2 K_0)^{-1} \left(\frac{D_{H,0}}{D_H}\right)^2 \frac{\partial\varepsilon}{\partial t^*}\,(x^*)^2. \tag{43}$$

Although in this case only the permeability term contributed to the pressure profile because of the relatively low Womersley number for normal breathing, the full form of Eq. (42) may be required for high-frequency breathing or perhaps in other applications where an expanding and contracting duct flow may be treated using the porous media approach described herein.

The velocity profiles are plotted in Fig. 3 with Fig. 3(a) showing line plots of the data for discrete time points and Fig. 3(b) showing a surface plot of the data over a complete breath cycle. Here it can be seen that at the time points $t^* = 1/4$ and $t^* = 3/4$, the velocity profile is zero everywhere since these times correspond to the maximum and minimum expansions, respectively, where the flow is in the process of reversing its direction. At $t^* = 0$ and $t^* = 1/2$ the velocity magnitudes are maximum since these times correspond to the peak expansion and contraction rates, respectively. Since outward flow is denoted as being positive, the velocity is negative at $t^* = 0$ and positive at $t^* = 1/2$. It is also observed that all profiles are linear with respect to x^* as implied by Eq. (41).

The pressure profiles are plotted in Fig. 4. These show a parabolic dependence of p^* on x^* as implied by Eq. (43). As would be expected, the same pressure profiles are observed at $t^* = 1/4$ (maximum duct size and porosity) and $t^* = 3/4$ (minimum duct size and porosity), since the fluid velocity is zero. Similarly, at the maximum expansion and contraction rates, occurring at $t^* = 0$ and $t^* = 1/2$, respectively, the maximum pressure magnitudes are attained.

Physically, these results show that under the present assumptions for alveolar expansion and contraction, the volume-averaged velocity profile is linearly related to the distance from the terminal alveolus, while the pressure is quadratically related. The shape of each profile is influenced by the instantaneous rate of change of porosity. The pressure profile is also influenced by the instantaneous duct size, as well as the dimensionless permeability and Womersley number.

3.5 Comparison to Poiseuille Flow Solution

Often, the pressure drop in airways is estimated based on the Poiseuille flow solution for flow in a circular cross-section duct (Kuwahara et al., 2009). Such models do not generally take into account the influence of alveoli, so it is of interest to determine the differences between this approach and the proposed model that does take into account the alveoli. According to the Poiseuille solution,

$$\frac{d\langle p\rangle^f}{dx} = -\frac{128\mu_f \dot{m}}{\rho_f \pi d^4}, \tag{44}$$

where $\dot{m}$ is the mass flow rate through the duct of diameter d. For one-dimensional flow with average velocity $\langle u\rangle$ over the cross section of the duct, the mass flow is

$$\dot{m} = \frac{\rho_f \langle u\rangle \pi d^2}{4}. \tag{45}$$

Combining Eqs. (44) and (45) results in

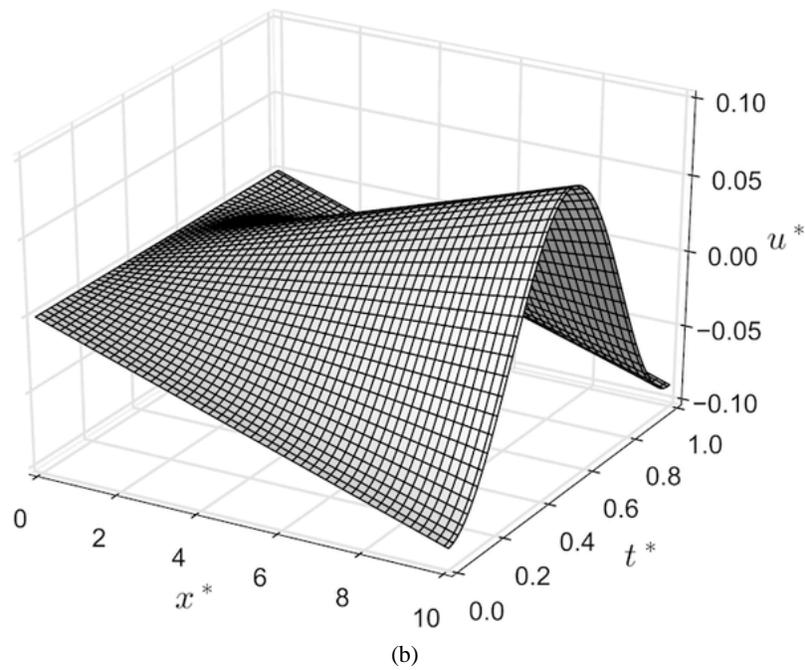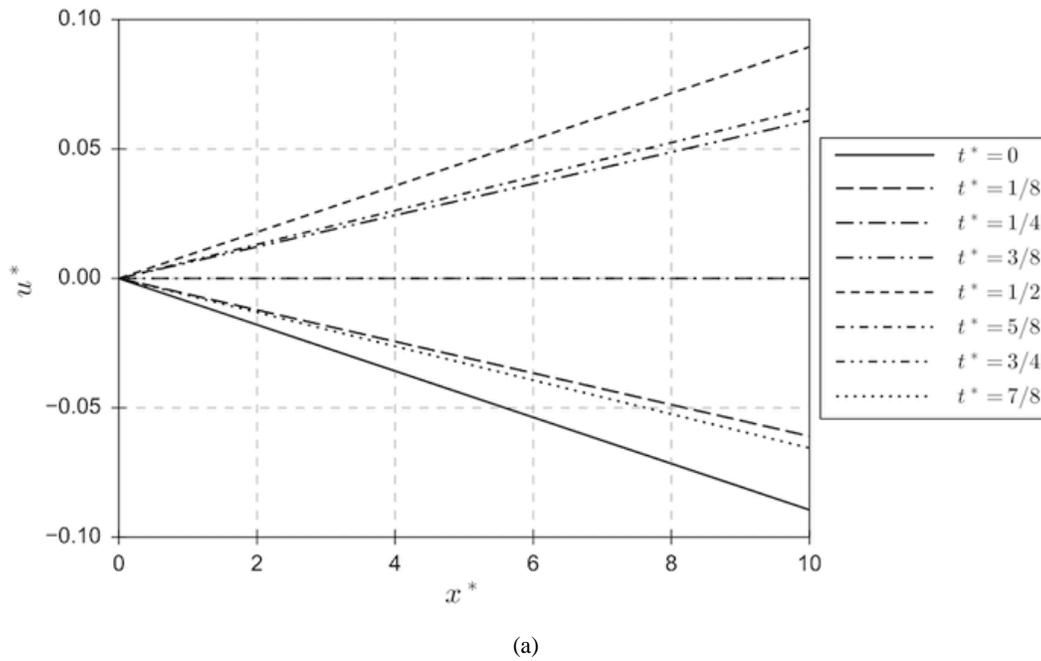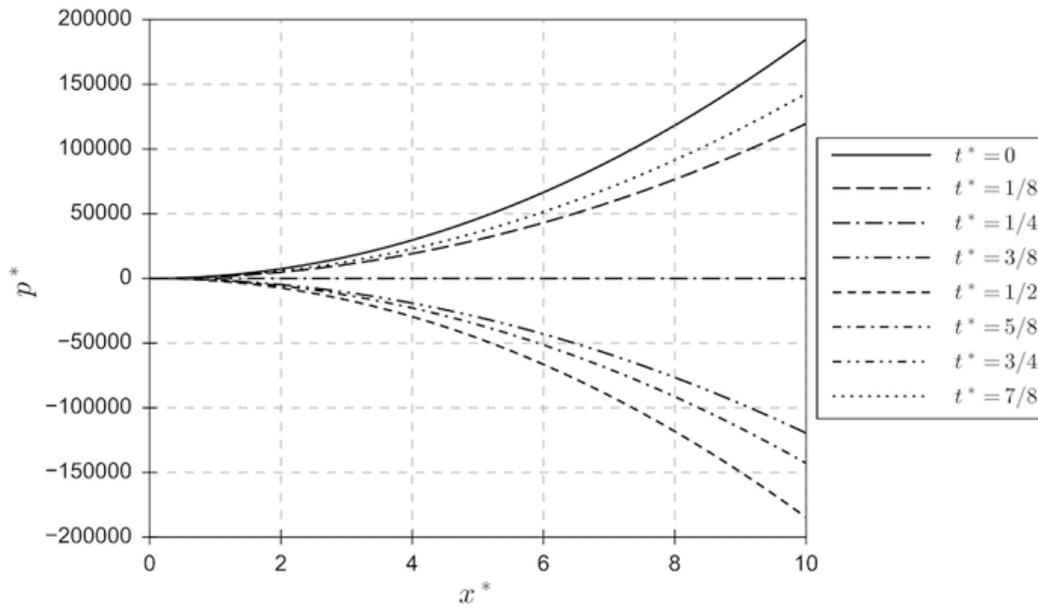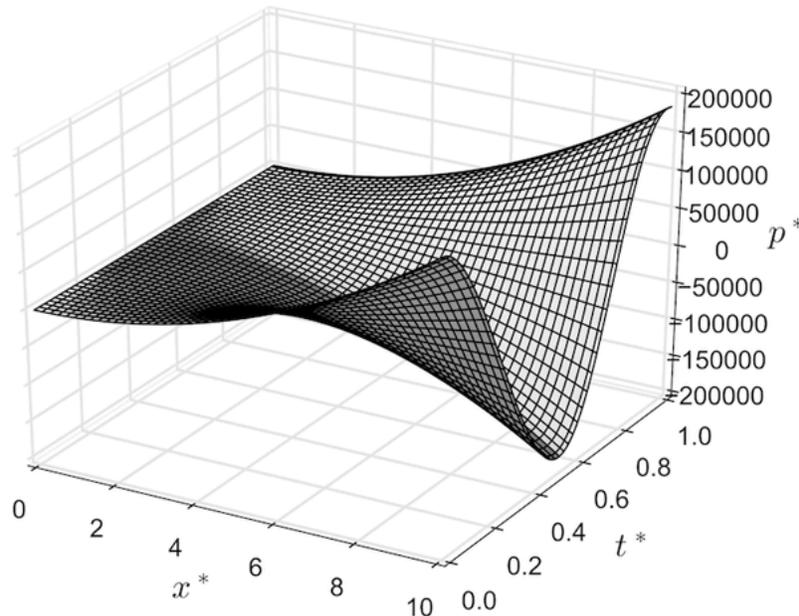$$\frac{d\langle p\rangle^f}{dx} = -\frac{32\mu_f \langle u\rangle}{d^2}. \tag{46}$$

(a)

(b)

FIG. 3: Plots of the dimensionless velocity as a function of the dimensionless coordinate x^* and the dimensionless time t^* for initial Womersley number Wo $= 0.01$, $\varepsilon_0 = 0.8$, and $\Lambda_{D_H} = 0.02329$

Equation (46) may be rewritten in dimensionless form using similar dimensionless variables as before except using the actual duct diameter in place of the hydraulic diameter. This results in

$$\frac{dp^*}{dx^*} = -\frac{8}{\text{Wo}^2}\left(\frac{d_0}{d}\right)^2 u^*. \tag{47}$$

(a)

(b)

FIG. 4: Plots of the dimensionless pressure p^* as a function of the dimensionless coordinate x^* and the dimensionless time t^* for initial Womersley number $\mathrm{Wo} = 0.01$, $\varepsilon_0 = 0.8$, and $\Lambda_{D_H} = 0.02329$

The equation for the dimensionless pressure gradient using the proposed model, assuming the permeability term to be dominant, is

$$\frac{\partial p^*}{\partial x^*} = -\frac{1}{4\varepsilon \mathrm{Wo}^2 K_0} \left(\frac{D_{H,0}}{D_H}\right)^2 u^*. \tag{48}$$

Comparing the two equations, we find a similar direct proportionality between the pressure gradient and the factor $(D_{H,0}/D_H)^2 u^*/\text{Wo}^2$, where in the case of the circular duct the hydraulic diameter is simply the duct diameter. Comparing the two equations further, it can be seen that the Poiseuille model would predict a value of K_0 equal to $(32\varepsilon)^{-1}$ which would not be a constant value due to the changing porosity. At an average porosity value of $\varepsilon = 0.8$, the Poiseuille model would predict $K_0 \approx 0.039$, which is substantially different from the value $K_0 = 0.00946$ predicted in this work. Therefore, this work suggests that the presence of alveoli surrounding a duct serves to decrease the permeability of the duct, which also corresponds to an increase in pressure drop. For an average porosity, this increase is more than fourfold. From a physical perspective it is believed that the increase in pressure drop arises from the increased energy dissipated within the recirculation zones that are maintained within the alveoli.

4. CONCLUDING REMARKS

A theoretically based closure model has been applied to the study of air flow in an alveolated duct. The closure model is based on the derivation of transport equations for the spatial deviations of velocity and pressure and the use of constitutive equations to transform these pore-level quantities into volume-averaged quantities. The transient nature of the flow as well as the spatially and temporally varying porosity causes some challenges; however, it is shown using rigorous scaling arguments that these factors may be ignored at the closure level and that the closure problem reduces to that for a fixed, constant porosity medium. The closure problem has been solved to obtain the permeability of the alveolated duct geometry, the scaling assumptions were verified using direct simulation of flow in an expanding and contracting alveolated duct, and some one-dimensional results for flow in an alveolated duct were presented. The key outcomes of this work are the permeability of the alveolated duct, which enables volume-averaged simulations to be conducted in large, three-dimensional regions of the lung parenchyma, as well as the simplified closure method which allows the permeability to be obtained for alveolated ducts in a straightforward manner.

ACKNOWLEDGMENTS

REFERENCES

Comerford, A., Förster, C., and Wall, W.A., Structured Tree Impedance Outflow Boundary Conditions for 3D Lung Simulations, *J. Biomech. Eng.*, vol. **132**, p. 081002, 2010.

DeGroot, C.T. and Straatman, A.G., Closure of Non-Equilibrium Volume-Averaged Energy Equations in High-Conductivity Porous Media, *Int. J. Heat Mass Transf.*, vol. **54**, pp. 5039–5048, 2011a.

DeGroot, C.T. and Straatman, A.G., A Finite-Volume Model for Fluid Flow and Non-Equilibrium Heat Transfer in Conjugate Fluid-Porous Domains using General Unstructured Grids, *Numer. Heat Transf., Part B*, vol. **60**, pp. 252–277, 2011b.

DeGroot, C.T. and Straatman, A.G., Numerical Results for the Effective Flow and Thermal Properties of Idealized Graphite Foam, *J. Heat Transf.*, vol. **134**, p. 042603, 2012.

DeGroot, C.T. and Straatman, A.G., A Conjugate Fluid-Porous Approach for Simulating Airflow in Realistic Geometric Representations of the Human Respiratory System, *J. Biomech. Eng.*, vol. **138**, p. 034501, 2016.

Gehr, P., Bachofen, M., and Weibel, E.R., The Normal Human Lung: Ultrastructure and Morphometric Estimation of Diffusion Capacity, *Respir. Physiol.*, vol. **32**, pp. 121–140, 1978.

Gemci, T., Ponyavin, V., Chen, Y., Chen, H., and Collins, R., Computational Model of Airflow in upper 17 Generations of Human Respiratory Tract, *J. Biomech.*, vol. **41**, pp. 2047–2054, 2008.

Gray, W.G., A Derivation of the Equations for Multi-Phase Transport, *Chem. Eng. Sci.*, vol. **30**, pp. 229–233, 1975.

Harding, E.M. and Robinson, R.J., Flow in a Terminal Alveolar Sac Model with Expanding Walls using Computational Fluid Dynamics, *Inhalation Toxicol.*, vol. **22**, pp. 669–678, 2010.

Hunter, J.D., Matplotlib: A 2D Graphics Environment, *Comput. Sci. Eng.*, vol. **9**, no. 3, pp. 90–95, 2007.

Kamschulte, M., Schneider, C.R., Litzbauer, H.D., Tscholl, D., Schneider, C., Zeiner, C., Krombach, G.A., Ritman, E.L., Bohle, R.M., and Langheinrich, A.C., Quantitative 3D Micro-CT Imaging of Human Lung Tissue, *Fortschr. Röntgenstr.*, vol. **185**, pp. 869–876, 2013.

Karl, A., Henry, F.S., and Tsuda, A., Low Reynolds Number Viscous Flow in an Alveolated Duct, *J. Biomech. Eng.*, vol. **126**, pp. 420–429, 2004.

Kaviany, M., *Principles of Heat Transfer in Porous Media*, 2nd ed., New York, NY: Springer-Verlag, 1995.

Kumar, H., Tawhai, M.H., Hoffman, E.A., and Lin, C.-L., The Effects of Geometry on Airflow in the Acinar Region of the Human Lung, *J. Biomech.*, vol. **42**, pp. 1635–1642, 2009.

Kumar, H., Tawhai, M.H., Hoffman, E.A., and Lin, C.-L., Steady Streaming: A Key Mixing Mechanism in Low-Reynolds-Number Acinar Flows, *Phys. Fluids*, vol. **23**, no. 4, p. 41902, 2011.

Kuwahara, F., Sano, Y., Liu, J., and Nakayama, A., A Porous Media Approach for Bifurcating Flow and Mass Transfer in a Human Lung, *J. Heat Transfer*, vol. **131**, 2009.

Lee, D.Y. and Lee, J.W., Characteristics of Particle Transport in an Expanding or Contracting Alveolated Tube, *J. Aerosol Sci.*, vol. **34**, pp. 1193–1215, 2003.

Li, Z. and Kleinstreuer, C., Airflow Analysis in the Alveolar Region using the Lattice-Boltzmann Method, *Med. Biol. Eng. Comput.*, vol. **49**, pp. 441–451, 2011.

Lin, C., Tawhai, M.H., Lennan, G.M., and Hoffman, E.A., Multiscale Simulation of Gas Flow in Subject-Specific Models of the Human Lung, *IEEE Eng. Med. Biol. Mag.*, vol. **28**, pp. 25–33, 2009.

Luo, H.Y. and Liu, Y., Modeling the Bifurcating Flow in a CT-Scanned Human Lung Airway, *J. Biomech.*, vol. **41**, pp. 2681–2688, 2008.

Ma, B. and Darquenne, C., Aerosol Deposition Characteristics in Distal Acinar Airways under Cyclic Breathing Conditions, *J. Appl. Physiol.*, vol. **110**, pp. 1271–1282, 2011.

Ma, B. and Lutchen, K.R., An Anatomically based Hybrid Computational Model of the Human Lung and its Application to Low Frequency Oscillatory Mechanics, *Ann. Biomed. Eng.*, vol. **34**, pp. 1691–1704, 2006.

Owen, M.R. and Lewis, M.A., The Mechanics of Lung Tissue under High-Frequency Ventilation, *SIAM J. Appl. Math.*, vol. **61**, pp. 1731–1761, 2001.

Saksono, P.H., Nithiarasu, P., and Sazonov, I., Numerical Prediction of Heat Transfer Patterns in a Subject-Specific Human upper Airway, *J. Heat Transf.*, vol. **134**, p. 031022, 2012.

Sznitman, J., Heimsch, F., Heimsch, T., Rusch, D., and Rösgen, T., Three-Dimensional Convective Alveolar Flow Induced by Rhythmic Breathing Motion of the Pulmonary Acinus, *J. Biomech. Eng.*, vol. **129**, pp. 658–665, 2007.

Sznitman, J., Heimsch, T., Wildhaber, J.H., Tsuda, A., and Rösgen, T., Respiratory Flow Phenomena and Gravitational Deposition in a Three-Dimensional Space-Filling Model of the Pulmonary Acinar Tree, *J. Biomech. Eng.*, vol. **131**, pp. 031010-1–16, 2009.

Tawhai, M.H. and Lin, C.-L., Image-based Modeling of Lung Structure and Function, *J. Magn. Reson. Imaging*, vol. **32**, pp. 1421–1431, 2010.

Tsuda, A., Henry, F.S., and Butler, J.P., Gas and Aerosol Mixing in the Acinus, *Respir. Physiol. Neuro.*, vol. **163**, pp. 139–149, 2008.

Walters, D.K. and Luke, W.H., A Method for Three-Dimensional Navier-Stokes Simulations of Large-Scale Regions of the Human Lung, *J. Fluids Eng.*, vol. **132**, p. 051101, 2010.

Walters, D.K. and Luke, W.H., Computational Fluid Dynamics Simulations of Particle Deposition in Large-Scale Multigenerational Lung Models, *J. Biomech. Eng.*, vol. **133**, p. 011003, 2011.

Weibel, E.R., *Morphometry of the Human Lung*, New York, NY: Springer-Verlag, 1963.

West, J.B., *Respiratory Physiology: The Essentials*, Baltimore, MD: Lippincott, Wiliams & Wilkins, 2008.

Whitaker, S., Diffusion and Dispersion in Porous Media, *AIChE J.*, vol. **13**, pp. 420–427, 1967.

Whitaker, S., The Forchheimer Equation: A Theoretical Development, *Transp. Porous Media*, vol. **25**, pp. 27–61, 1996.

Yin, Y., Choi, J., Hoffman, E.A., Tawhai, M.H., and Lin, C.-L., Simulation of Pulmonary Air Flow with a Subject-Specific Boundary Condition, *J. Biomech.*, vol. **43**, pp. 2159–2163, 2010.

Zhang, Z. and Kleinstreuer, C., Transient Airflow Structures and Particle Transport in a Sequentially Branching Lung Airway Model, *Phys. Fluids*, vol. **14**, pp. 862–880, 2002.

Zhang, Z. and Kleinstreuer, C., Species Heat and Mass Transfer in a Human upper Airway Model, *Int. J. Heat Mass Transf.*, vol. **46**, pp. 4755–4768, 2003.

Zhang, Z., Kleinstreuer, C., and Kim, C.S., Airflow and Nanoparticle Deposition in a 16-Generation Tracheobronchial Airway Model, *Ann. Biomed. Eng.*, vol. **36**, pp. 2095–2110, 2008.